ACTA ONCOLOGICA
2021, VOL. 60, NO. 2, 199–206
https://doi.org/10.1080/0284186X.2020.1817547

Taylor & Francis
Taylor & Francis Group

ORIGINAL ARTICLE

Robust treatment planning of dose painting for prostate cancer based on ADC-to-Gleason score mappings – what is the potential to increase the tumor control probability?

Eric Grönlund[a,b], Erik Almhagen[a,c], Silvia Johansson[d,e], Erik Traneus[f], Tufve Nyholm[g], Camilla Thellenberg[g] and Anders Ahnesjö[a,d]

[a]Medical radiation sciences, Department of Immunology, Genetics and Pathology, Uppsala University, Uppsala, Sweden; [b]Section of Medical Physics, Eskilstuna Hospital, Eskilstuna, Sweden; [c]The Skandion Clinic, Uppsala, Sweden; [d]Uppsala University Hospital, Uppsala, Sweden; [e]Experimental and clinical oncology, Department of Immunology, Genetics and Pathology, Uppsala University, Uppsala, Sweden; [f]RaySearch Laboratories, Stockholm, Sweden; [g]Department of Radiation Sciences, Umeå University, Umeå, Sweden

ABSTRACT

Background and purpose: The aim of this study was to evaluate the potential to increase the tumor control probability (TCP) with 'dose painting by numbers' (DPBN) plans optimized in a treatment planning system (TPS) compared to uniform dose plans. The DPBN optimization was based on our earlier published formalism for prostate cancer that is driven by dose-responses of Gleason scores mapped from apparent diffusion coefficients (ADC).

Material and methods: For 17 included patients, a set of DPBN plans were optimized in a TPS by maximizing the TCP for an equal average dose to the prostate volume (CTVT) as for a conventional uniform dose treatment. For the plan optimizations we applied different photon energies, different precisions for the ADC-to-Gleason mappings, and different CTVT positioning uncertainties. The TCP increasing potential was evaluated by the DPBN efficiency, defined as the ratio of TCP increases for DPBN plans by TCP increases for ideal DPBN prescriptions (optimized without considering radiation transport phenomena, uncertainties of the CTVT positioning, and uncertainties of the ADC-to-Gleason mapping).

Results: The median DPBN efficiency for the most conservative planning scenario optimized with a low precision ADC-to-Gleason mapping, and a positioning uncertainty of 0.6 cm was 10%, meaning that more than half of the patients had a TCP gain of at least 10% of the TCP for an ideal DPBN prescription. By increasing the precision of the ADC-to-Gleason mapping, and decreasing the positioning uncertainty the median DPBN efficiency increased by up to 40%.

Conclusions: TCP increases with DPBN plans optimized in a TPS were found more likely with a high precision mapping of image data into dose-responses and a high certainty of the tumor positioning. These findings motivate further development to ensure precise mappings of image data into dose-responses and to ensure a high spatial certainty of the tumor positioning when implementing DPBN clinically.

ARTICLE HISTORY
Received 29 January 2020
Accepted 26 August 2020

KEYWORDS
Dose painting; dose painting by numbers; prostate cancer; apparent diffusion coefficient MRI

Introduction

More than half of the patients diagnosed with prostate cancer in Sweden receive radiotherapy (RT) [1], which in combination with endocrine therapy is the preferred treatment for high-risk patients [2]. The risk for relapse can be mitigated by allowing for dose escalation to increase the tumor control probability (TCP) [3–8]. Local recurrences after RT has been demonstrated to often occur at the same spatial location as the site of the primary tumor [9]. However, dose escalation comes with the expense of increasing the risk for a normal tissue complication probability (NTCP) [5,6,10]. To reach a better tradeoff between a high TCP and a low NTCP dose painting has been proposed [11]. The aim of dose painting is to increase the TCP to NTCP ratio through prescribing and delivering nonuniform dose distributions based on spatially varying dose-responses derived from functional imaging data.

One of the most predictive factors for prostate cancer prognosis is the Gleason score determined from biopsy samples of prostate tissue. It has been shown that increasing Gleason scores correlate with an increased risk for biochemical recurrences after both RT and prostatectomy [12–15]. Ghobadi et al. [16] hypothesized that Gleason scores could be used to characterize patient specific dose-responses through implementing Gleason scores as a parameter in the

CONTACT Eric Grönlund eric.gronlund@regionsormland.se Section of Medical Physics, Eskilstuna Hospital, Medicinsk fysik och teknik, Mälarsjukhuset, Eskilstuna 631 88, Sweden

Supplemental data for this article is available here.

linear-quadratic model. In their modeling study, they found that the prostate dose could be differentiated by 10 Gy with an equal TCP as for uniform dose treatments. Furthermore, increasing Gleason scores are shown to correlate with decreasing apparent diffusion coefficient (ADC) data acquired from diffusion weighted MR imaging [17–23]. Similar to Ghobadi et al. [16], we hypothesized in our earlier study [24] that Gleason scores could be used to predict differentiated dose-responses and thus used to maximize the TCP with the average dose constrained to that for conventional uniform dose treatments. The underlying Gleason driven dose-response functions were derived from a learning set of pre-RT Gleason scores and post-RT outcomes from 122 high-risk patients treated with a uniform dose of 91.6 Gy EQD_2. The endpoint for TCP was freedom from biochemical recurrences (BCR) 5-years post-RT.

In our previously published DPBN formalism [24] we derived heterogeneous dose painting prescriptions based on image predicted dose-responses to maximize the TCP per used radiant energy. We did so without considering any practical circumstances for safe delivery such as geometrical uncertainties or dose gradient limitations from particle transport physics, etc. The resulting TCP increases as compared with a uniform dose treatment, yielded thus a theoretical limit for the maximal gain with DPBN. In this study we have implemented our earlier dose painting formalism [24] into a treatment planning system (TPS) considering delivery limitations with the aim to evaluate the feasibility to actualize the potential TCP increases with optimized dose painting by numbers (DPBN) plans in comparison to uniform dose treatments for high-risk prostate cancer. We implemented the DPBN optimization to be feasible with minimax optimization without need for specification of explicit margins or PTV to ensure robustness of the TCP and the dose distribution regarding uncertainties of the iso-center positioning. Several aspects of the data processing and treatment planning/delivery steps were explored in order to establish which parameters are of importance for implementing a feasible DPBN workflow amiable for clinical implementation. These aspects include the precision of ADC to Gleason mapping, choice of photon beam energy and different scenarios for positioning uncertainties during dose delivery.

Material and methods

We tested 12 different planning conditions on a test set of 17 patients to evaluate the tested conditions impact on the result, considering various uncertainties and the limitations of physically deliverable doses. The DPBN formalism is driven by Gleason score dependent dose-response functions derived from a learning set consisting of pre-RT Gleason scores and post-RT outcomes, as described earlier [24]. Moreover, the ADC driven dose painting is enabled through mapping ADC image data to the Gleason driven dose-responses by means of probability density functions derived from published correlations between Gleason scores and ADC data given by Turkbey et al. [17]. As endpoint for TCP we used the 5-year freedom from bio-chemical recurrences.

Patient data

As test set for this study we used data from 17 patients out of the 18 high-risk patients we used in our previous study [24]. All included patients had been imaged with diffusion weighted MR-imaging before androgen deprivation therapy to provide ADC images unaffected of hormonal induced changes of the prostate tissues. The ADC images were for some patients acquired with a 1.5 Tesla MRI camera from Siemens, where the ADC image data were resolved with three values of the diffusion weighting parameter ('b-value'), 0, 160 and 800 s/mm^2. For the remaining patients a 3.0 Tesla PET/MRI camera from GE Healthcare was used, with two b-values of 200 and 800 s/mm^2. For each patient the ADC images were rigidly registered to the CT images used for treatment planning. The contours of each patient had been segmented on the CT image sets according to clinical protocols. In our earlier study [24], we did small manual modifications of each patient's segmented target prostate volume (CTVT) to yield a better match of the ADC maps with the CT based CTVT segmentations. However, to align this study toward a more realistic clinical setting we did not perform any modifications of the segmented CTVTs. One patient was hence excluded from the original set of 18 patients because of a large anatomical difference of the rectum between the CT and ADC image sets, which yielded that the CTVT defined on the CT image set was biased to enclose ADC data from the rectum. All 17 included patients constituted a subset of the patients treated with RT in the PARAPLY phase 2 trial (ClinicalTrials.gov Identifier NCT01962324; Umeå board ethical approval reference numbers 2013/154-31 and 2015/75-32).

DPBN treatment plan efficiency

The realistic potential of TCP increases with DPBN plans was evaluated in comparison to the TCP increases for ideal DPBN prescriptions (i.e., doses assigned to each voxel by neglecting radiation transport phenomena and uncertainties of the mapping of ADC-to-Gleason score). This potential was evaluated as the DPBN efficiency (η_{DPBN}) given as

$$\eta_{\mathrm{DPBN}} = \left(\frac{\mathrm{TCP}_{\mathrm{real}} - \mathrm{TCP}_{\mathrm{hom}}}{\mathrm{TCP}_{\mathrm{ideal}} - \mathrm{TCP}_{\mathrm{hom}}}\right), \quad (1)$$

where $\mathrm{TCP}_{\mathrm{real}}$, $\mathrm{TCP}_{\mathrm{hom}}$ and $\mathrm{TCP}_{\mathrm{ideal}}$ correspond to the TCP for realistic DPBN plans, the TCP for a homogeneous conventional dose and the TCP for ideal DPBN prescriptions, respectively. Both the ideal DPBN prescriptions and the realistic DPBN plans were optimized under the assumption of voxel independency through maximizing the product of the TCP for each voxel within the CTVT, see Equation (3). Furthermore, to avoid too high doses we constrained the average CTVT dose to 91.6 Gy EQD_2 (i.e., the uniform treatment dose for the original learning set [24] with $\alpha/\beta = 1.93$ Gy according to Vogelius et al. and Casares-Magaz et al. [25,26]). To acquire a theoretical maximum TCP gain for the ideal DPBN prescriptions we assumed that the ADC data could be exactly mapped to the mean Gleason score per ADC value without any probabilistic spread, i.e., a direct one-

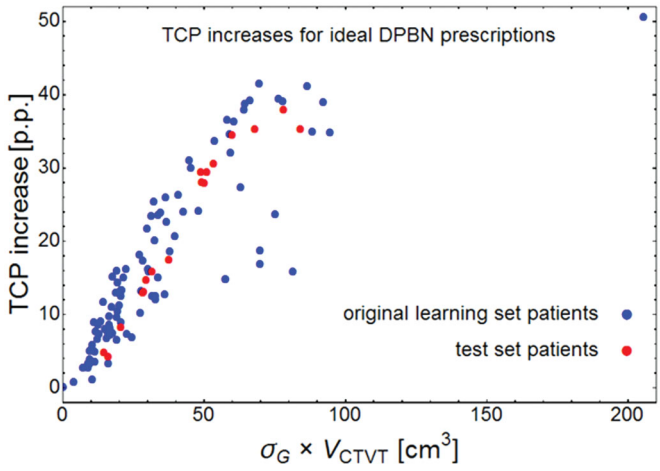

Figure 1. TCP increases for ideal dose painting prescriptions both for the original learning set patients (blue dots) and for the test set patients included in this study (red dots). These TCP increases are plotted vs. the standard deviation of Gleason scores multiplied by the prostate CTVT volumes as in our earlier study where we found this measure to correlate well with a TCP increase [24]. Note that the TCP increases for the test set patients (red dots) are not the same TCP increases as given in our earlier study [24]. This is because the test set patients' ideal dose painting prescriptions are in this study based on a direct one-to-one mapping of ADC-to-Gleason scores and based on the clinically determined segmentations of the CTVTs without any manual modifications (as we did in our previous study).

to-one mapping of ADC data into a Gleason score. This is in contrast to our previous study [24] where the DPBN prescriptions for the test set patients were optimized with a conditional probability map based on the uncertainty ranges given by the study from Turkbey et al. [17], i.e., the low precision mapping described in section 2.4. In Figure 1 we show the TCP increases (i.e., $TCP_{ideal} - TCP_{hom}$) resulting from each test set patients ideal DPBN prescription where we also show the TCP increases for the learning set given in our previous study [24].

TCP modeling and optimization

The ADC driven dose painting was enabled through translating ADC image data into Gleason score dose-response functions based on published correlations between Gleason scores and ADC data given by Turkbey et al. [17]. The assumption behind this translation was that the TCP for a voxel could be expressed as the probability weighted geometric average over the probability distribution of Gleason scores for the voxel as

$$\mathrm{TCP}_{\mathrm{vox}}\left(D_{\mathrm{EQD}_{2\mathrm{Gy}}}\right) = \left(\prod_{j=1}^{j_{\max}} \left(\mathrm{TCP}_{\mathrm{vox}}\left(D_{\mathrm{EQD}_{2\mathrm{Gy}}}, G_j\right)\right)^{P\left(G_j(ADC)\right)\Delta G}\right)^{f_{\mathrm{vox}}} \tag{2}$$

where $\mathrm{TCP}_{\mathrm{vox}}(D_{\mathrm{EQD}_{2\mathrm{Gy}}}, G_j)$ is the Gleason score driven dose-response for an EQD_2 voxel dose $D_{\mathrm{EQD}_{2\mathrm{Gy}}}$ and Gleason score G_j, $P(G_j(ADC))\Delta G$ is the conditional probability map that gives the probability for G_j, with interval width ΔG, based on the voxel's apparent diffusion coefficient ADC, and f_{vox} is the fraction of the voxel that is within the CTVT, i.e., $0 < f_{vox} \leq 1$. The derivation of the Gleason driven dose-responses $\mathrm{TCP}_{\mathrm{vox}}(D_{\mathrm{EQD}_{2\mathrm{Gy}}}, G_j)$ and the conditional probability map $P(G_j(ADC))\Delta G$ is given in our earlier paper [24]. The formalism was implemented as a planning objective into a research version of the treatment planning system (TPS) RayStation. The optimization framework of the TPS is designed to minimize scalar objectives, so we formulated the planning objective as

$$\underset{d}{\text{minimize}} \quad 1 - \prod_{\mathrm{vox}\in\mathrm{CTVT}} \left(\mathrm{TCP}_{\mathrm{vox}}\left(D_{\mathrm{EQD}_{2\mathrm{Gy}}}(d)\right)\right) \tag{3}$$

where $\mathrm{TCP}_{\mathrm{vox}}(D_{\mathrm{EQD}_{2\mathrm{Gy}}}(d))$ is given by Equation (2) as a function of the voxel dose $D_{\mathrm{EQD}_{2\mathrm{Gy}}}$ determined from the physical dose distribution d with $\alpha/\beta = 1.93$ Gy [25,26]. We used the planning objective of Equation (3) in the robust minimax optimization framework of the TPS [27,28] for which the optimization problem can be formulated as

$$\begin{aligned} \underset{d}{\text{minimize}} \quad & \left(\max_k \left[\sum_{i=1}^{n} w_i f_i(d_k)\right] + \sum_{i=n+1}^{n+m} w_i f_i(d)\right) \\ \text{subject to} \quad & \begin{cases} c_q(d_k) \leq 0, & \begin{cases} q = 1, \ldots, Q \\ k = 1, \ldots, K \end{cases} \\ c_j(d) \leq 0, & j = 1, \ldots, J, \end{cases} \end{aligned} \tag{4}$$

where f_i is the $i-$th planning objective with importance weight w_i, n is the number of objectives used with minimax optimization, m is the number of objectives used without minimax optimization, Q is the number of dose constraints c_q used with minimax optimization, and J is the number of dose constraints c_j used without minimax optimization. The robust minimax part of the optimization minimizes the maximum objective value selected from K scenarios of iso-center positioning errors (that yields the dose error scenarios d_k) and hence ensures a geometrically robust dose coverage to the tumor target volume without the use of a PTV [27,28].

Table 1. The different settings for the plan optimizations, where the photon energy, precision on the mapping of ADC→Gleason scores, and the robustness distance were varied, yielding a total of 12 plans per patient.

Photon energy [MV]	Mapping of ADC→Gleason score Low precision (LP) or High precision (HP)	Robustness distance [cm]
6	LP	0.0
6	LP	0.2
6	LP	0.6
6	HP	0.0
6	HP	0.2
6	HP	0.6
15	LP	0.0
15	LP	0.2
15	LP	0.6
15	HP	0.0
15	HP	0.2
15	HP	0.6

Setup of dose painting plans

For each patient we created a total of 12 DPBN volumetric-modulated arc therapy (VMAT) plans with 2 arcs completing a full rotation for a Versa HD™ linear accelerator and the dose grid set with $3.0 \times 3.0 \times 3.0\,\mathrm{mm}^3$ voxels. See Table 1 for a summary of the tested conditions for the 12 different plans. To test whether variations in lateral dose resolution due to different photon energies would affect the DPBN optimization we optimized six plans with 6 MV photons and

six plans with 15 MV photons. Out of the six plans per photon energy, three were optimized with a low precision (LP) conditional probability map, i.e., the original conditional probability map from our earlier study [24], which was constructed from the Gleason-to-ADC correlations given by Turkbey et al. [17]. The other three plans were optimized with a high precision (HP) conditional probability map, which were constructed by compressing the interquartile range data from Turkbey et al. [17] to instead be contained in the range from 12.5 to 87.5%. Furthermore, we chose to optimize with robust minimax optimization for three levels of isocenter positioning errors for the set of plans optimized with the LP and the HP conditional probability map, respectively. The isocenter positioning errors were tested by three different settings: 0.6 cm corresponding to the conventional CTV-to-PTV margin used in the PARAPLY study; 0.2 cm to simulate a very high precision treatment that only take into account the uncertainty of intra-fractional movement of the prostate (based on the recommended margin from Kotte et al. [29]); and finally without any isocenter positioning errors for use as a reference.

For all plans we chose to use 35 fractions where the baseline dose $D_{98\%}$ to the CTVT should not be less than 77 Gy and the maximum dose not should exceed the boost dose of 95 Gy, as used in the FLAME trial [30,31]. Furthermore, as in our previous study [24] we considered that the average dose of 91.6 Gy EQD_2 should be kept equal for the CTVT, which for 35 fractions and $\alpha/\beta = 1.93$ Gy [25] equals 83.4 Gy (physical dose). Moreover, to prevent the dose painting optimization to yield hot-spots to the region surrounding the edge of the CTVT we added planning objectives for the CTVT-to-PTVT margin volume with a weighting factor such that the volume's dose distribution become similar to that for conventional uniform dose treatments. The prescription doses for the therapeutic pelvic lymphatic nodes (PTVN-T) and for the prophylactic nodes (PTVN-P) were set to 70 Gy and 56 Gy, respectively. See Table A1 in the Supplementary Appendix for details of the used objectives and constraints for the optimization of DPBN plans.

Results

As expected, ideal DPBN prescriptions demonstrates a greater potential for TCP increases than TCP increases for realistic DPBN plans, see Figure 1 in comparison to the left panels of Figure 2. The TCP gains for the ideal DPBN prescriptions (Figure 1) correlated with the standard deviation of Gleason scores multiplied by the CTVT volumes ($\sigma_G \times V_{CTVT}$), meaning that heterogeneous and large prostate volumes possess a larger potential for TCP increases than for homogeneous and smaller prostate volumes (as shown in our earlier study [24]). However, this correlation was much less pronounced for the TCP increases of the realistic DPBN plans optimized under various conditions (Figure 2). In Table A2 in the Supplementary Appendix is the patient groups' average TCP increases listed for the 12 different planning scenarios. The DPBN plans that demonstrated the greatest potential for TCP increases were those reflecting very high precision irradiation, i.e., the non-robustly optimized plans with the high precision conditional probability ADC-to-Gleason map, and the plans that demonstrated the lowest potential were the most robust plans (i.e., the plans optimized to be robust for an iso-center positioning error of at most 0.6 cm) optimized with the original (low precision) ADC to Gleason probability map. It was also found that the effect of optimizing with 6 MV photons did not yield any significant TCP increase as compared to optimizing with 15 MV photons (see Table A2 in the Supplementary Appendix).

The DPBN efficiency for the different planning scenarios was evaluated with Equation (1) to give a measure of the realistic potential to actualize TCP increases inherently available for dose painting under ideal conditions. In Figure 3 we demonstrate the DPBN efficiency for all different planning setups, where it is shown that a decrease of the robustness distance and an increase of the precision to map ADC-to-Gleason scores yields a higher DPBN efficiency. However, some plans had a negative DPBN efficiency, meaning that these DPBN plans had a lower TCP than for a uniform dose treatment. Nevertheless, the 25th percentile of the DPBN efficiency for all planning scenarios all had a positive efficiency meaning that at least 75% of the DPBN plans yielded a greater TCP than the TCP for a uniform dose treatment. See Figure 3 for the numerical range of the DPBN efficiency of each plan optimization.

The resulting DPBN plan doses versus ADC data are shown in Figure 4 for one of the patients, where for comparison also the ideal DPBN prescription dose is shown (i.e., voxel doses optimized for the CTVT without considering radiation transport phenomena or geometric uncertainties).

Discussion

The basic idea of dose painting is to widen the therapeutic window through prescribing non-uniform doses based on dose-response predictors mapped from functional image data. Based on several studies demonstrating that increasing Gleason scores correlate with decreasing ADC data [17–23], albeit with inherent uncertainties, we have constructed a dose painting formalism where ADC data is mapped to Gleason score driven dose-responses as outlined in Equation (2). The data we used for mapping of ADC data to Gleason scores [17] report how Gleason scores correlate with ADC, whereas our formalism needs the mapping of ADC-to-Gleason scores instead, forcing us to reconstruct the inverse of the reported data. It would be more appealing to use data that directly correlate ADC-to-Gleason scores, but such detailed studies are not yet available to our knowledge. The ADC images for our test set patients may not be fully comparable to the ADC images used by Turkbey et al. [17]. However, because the presented dose painting formalism in practice redistribute the integral dose available for the prostate volume it is rather the relative distribution of ADC values within the prostate than the absolute ADC values that affect the dose optimization.

Higher accuracy of the ADC-to-Gleason score mapping can potentially improve the benefit of DPBN (see Figure 2),

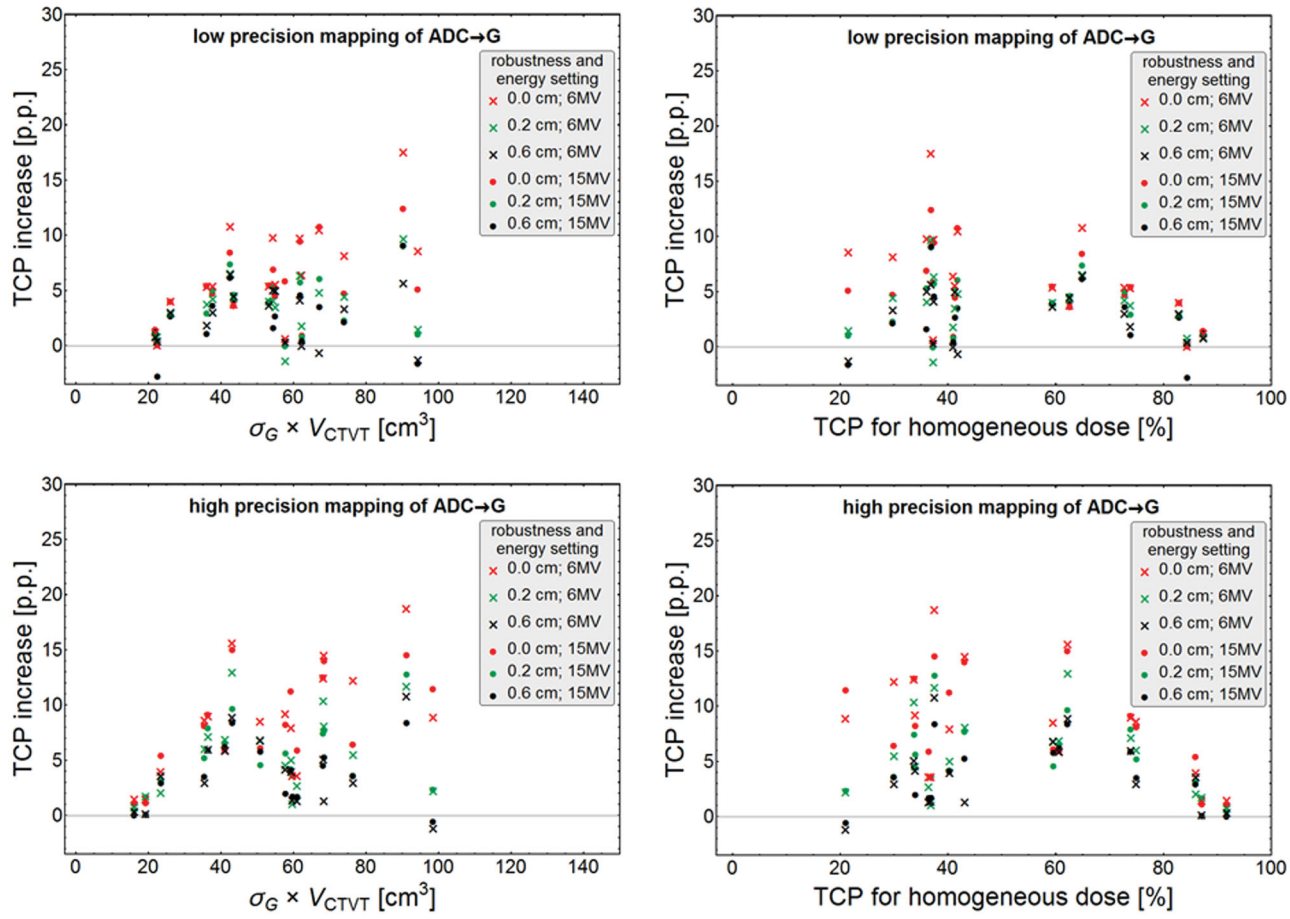

Figure 2. The panels in the left column show TCP increases per patient with realistic DPBN vs. the standard deviation of Gleason scores multiplied by the CTVT volumes, whereas the panels in the right column demonstrate the TCP increases vs. the TCP for a uniform dose. The rows differentiate the plans optimized with the low precision conditional probability map (uppermost) and with the high precision conditional probability map (lowermost). The colors demonstrate the used distances for robust minimax optimization, red without any iso-center displacements, green a maximum iso-center displacement of 0.2 cm and black a maximum iso-center displacement of 0.6 cm.

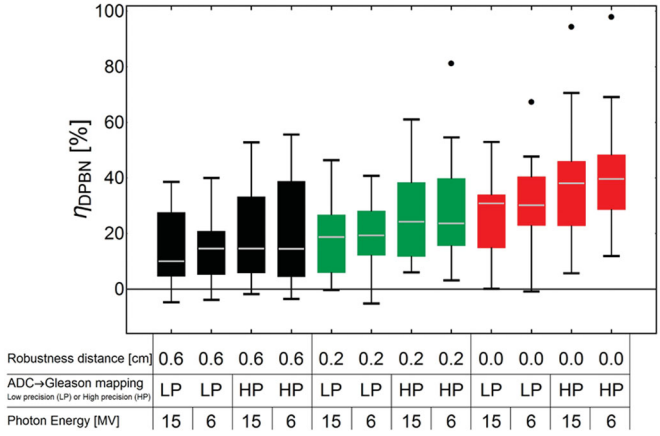

Figure 3. Box and whisker plots of the resulting efficiency to increase the TCP for the test set patients in different planning scenarios as compared to the ideal DPBN prescriptions. Along the abscissa are the planning settings differentiated with the used isocenter displacements for minimax optimization (black-0.6 cm, green-0.2 cm, red without robust optimization), the precision on the ADC→Gleason mappings (LP-low precision, HP-high precision), and the photon energies (15 MV and 6 MV). The box center line corresponds to the median, the box range 25th to 75th percentile, the whiskers show the data within 1.5 interquartile range, and the dots correspond to outliers.

primarily because when high Gleason score regions are better resolved the optimizer can use the available dose spending budget more effectively. For future development of DPBN, it is hence important to accurately and with a high precision localize the most aggressive tumor voxels. The study from Borren et al. [32] demonstrate that multi-parametric MR-imaging can be a helpful tool to locate the most aggressive tumor voxels. However, limitations in resolution of clinical dose delivery puts a limit to what can be targeted. Possible presence of high malignancy regions not resolved in the images will have a negligible impact on the planned dose distribution but will cause the predicted TCP increase to be overestimated.

We hypothesized that a lower photon energy of 6 MV would yield greater TCP increases than for a higher photon energy of 15 MV, because a lower energy implies a narrower penumbra that hence may yield a better formation of heterogeneous dose painting distributions. However, the different photon energies did not impact the TCP increase potential as much as the other tested factors, i.e., the mapping precision and the robustness distance (Figure 2,3 and Table A2 in the Supplementary Appendix).

The potential to increase the TCP for realistic treatment techniques is illustrated in Figure 2 where the plans optimized with the maximum positioning precision (i.e., zero robustness distance) indicated larger potential to increase

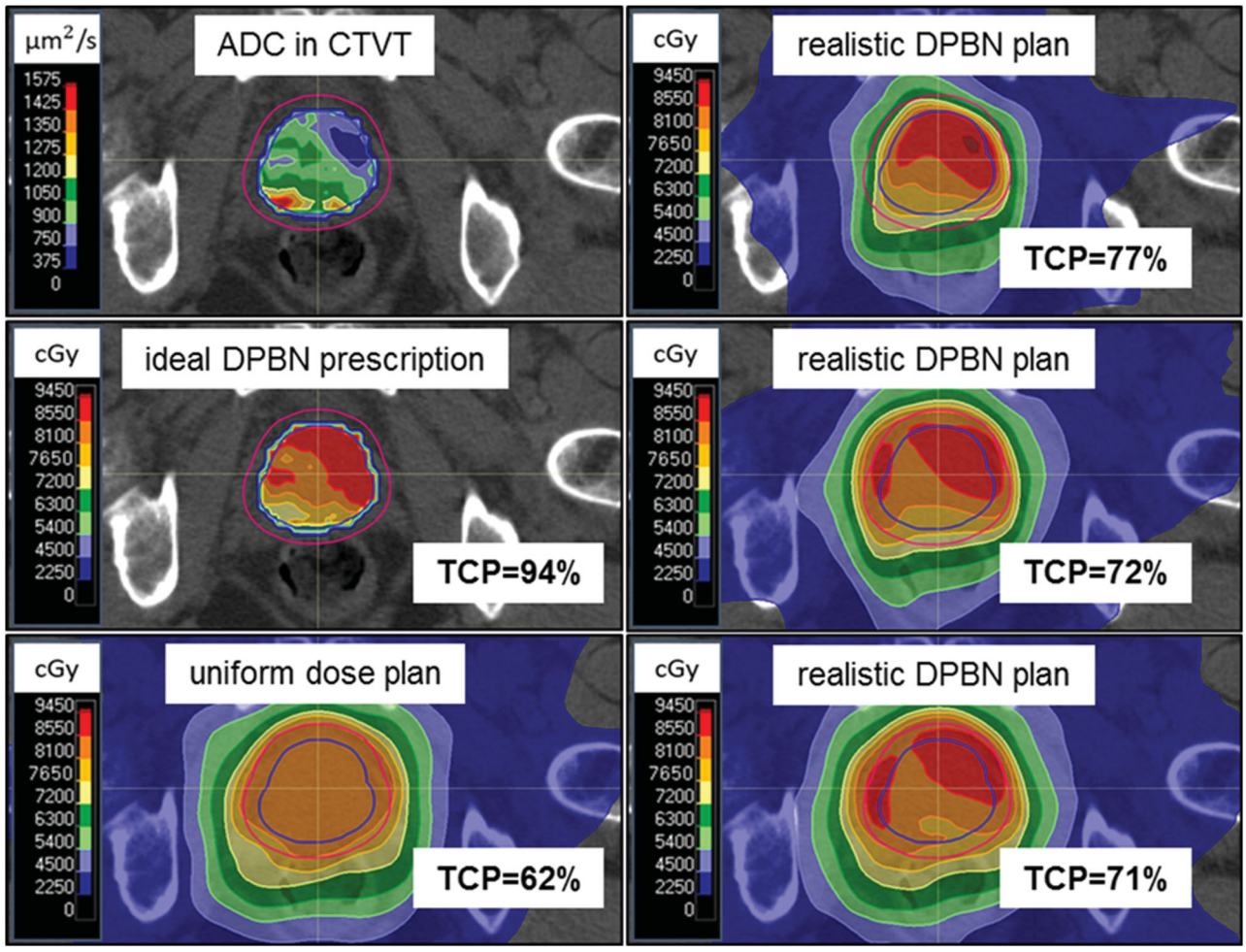

Figure 4. Illustration of different dose plans for a CT-image slice for one of the patients. The blue contour marks the prostate target volume (CTVT) and the red contour the PTVT made with a margin of 6 mm from the CTVT. (Upper left) ADC image data within the CTVT. (Middle left) the ideal DPBN prescription, where the low-ADC regions are prescribed a higher dose than the high-ADC regions with a lower dose. (Lower left) A dose plan optimized to be uniform for the PTVT. (Upper right) A DPBN plan optimized with 15 MV photons, high precision (HP) mapping of ADC→Gleason scores and without iso-center displacements. (Middle right) A DPBN plan optimized with 15 MV photons, HP mapping of ADC→Gleason scores and with minimax robust optimization for a maximum isocenter displacement of 2 mm. (Lower right) A DPBN plan optimized with 15 MV photons, HP mapping of ADC→Gleason scores and with minimax robust optimization for a maximum iso-center displacement of 6 mm.

the TCP than the plans optimized with larger distances. This is expected since the non-robust plans can reach dose distributions more similar to the ideal DPBN prescriptions than the plans optimized with non-zero robustness distances.

We did a robustness test of the planned TCP for one of the patients through sampling a large number of treatment scenarios with random isocenter displacements for each scenario. For the plans optimized without considering robustness, it was found that the TCP varied greatly for each sampled scenario, whereas the plans optimized with a robustness of either 0.2 cm or 0.6 cm had a TCP increase that was very robust for all sampled scenarios.

Our approach to reach a plan with a robust TCP by utilizing minimax optimization is in contrast to other studies such as Sterpin et al. and Witte et al. [33,34] that aimed toward a robust dose distribution by including random and systematic errors in the optimization process. Nevertheless, another approach from Witte et al. [35] share similarities with ours by striving for a robust maximization of the expectation value for the TCP. In their study [35] they included random and systematic uncertainties and utilized a Poisson dose-response modeling for the TCP maximization, whereas we instead utilized minimax optimization to ensure that the worst-case TCP value for an iso-center displacement reaches as high value as possible. Furthermore, through using minimax optimization it was found that the peripheral doses of the CTVT close to the surrounding normal tissues was increasing, which motivated our planning objective for the shell volume of the CTVT-to-PTVT (see Table A1 in the Supplementary Appendix).

The ideal DPBN prescriptions demonstrated an increase of the TCP as compared to a uniform dose for all patients, see Figure 1. The realistic potential to actualize these TCP increases was evaluated through the DPBN efficiency, calculated by Equation (1) and shown in Figure 3. A DPBN efficiency of 100% would imply a perfect realization of the ideal DPBN prescriptions, which as expected not was the case, see Figure 3. We found that the DPBN efficiency was decreasing with an increasing robustness, with a median DPBN efficiency of 10% for 0.6 cm robustness. For this robustness

setting of 0.6 cm it can hence be expected that more than 50% of the patients will have a TCP increase of at least 10% of the TCP increase for an ideal DPBN prescription.

Clinical trials are needed to prove that dose painting actually increases the prospects for prostate cancer patients in comparison to conventional treatments. Furthermore, our DPBN formalism focuses only on the prostate target volume (CTVT) and not on the seminal vesicles which were planned toward a homogeneous dose (see Table A1 in the Supplementary Appendix). Even though dose painting not yet has been proven to increase the prospects for prostate cancer patients, studies such as the ASCENDE RT trial have shown that general boost treatments can increase the TCP [8]. The ASCENDE RT trial demonstrated that the 5-year freedom from a biochemical recurrence increased by 4.8 p.p. for the boost treated patients as compared the control group which is similar to the numbers presented in Table A2 in the Supplementary Appendix. Furthermore, the FLAME trial aims to provide with knowledge whether dose painting may be beneficial [31]. In FLAME multi-parametric MRI was used to distinguish primary tumor regions that for 35 fractions received a boost dose dose of 95 Gy and with 77 Gy to the rest of the prostate volumes [31]. While the clinical outcomes for the FLAME trial not have been published yet, it has been shown that the toxicity rates for the boost-treated patients not increased compared to the control group treated with a conventional uniform dose [30]. Moreover, we used the same dose range for the CTVT as in the FLAME trial (i.e., 77 Gy – 95 Gy) for the DPBN plan optimization, with an extra inclusion of the mean dose constraint of 83.4 Gy (see Table A1 in the Supplementary Appendix). It is hence likely that the DPBN plans we have optimized are safe for patient delivery with respect to the NTCP for organs at risk.

Conclusions

We have in this planning study evaluated the potential to clinically actualize prognosticated TCP increases from ideal redistributions of homogeneous doses within the CTV. We used a dose painting formalism that maps ADC data into dose-responses driven by Gleason scores for TCP determination. For evaluation we used a commercial TPS with tools for robust minimax optimization and a number of different settings were used to emulate different clinically realistic dose plans. We concluded that robust minimax optimization is feasible for DPBN using TCP modeling from ADC images, although it was not possible to reach the prognosticated TCP increases from ideal dose redistributions. Of the investigated factors; photon beam energy: ADC mapping accuracy: and positional accuracy, we concluded that the positional accuracy was most important, and that with increasing positional accuracy the ADC mapping accuracy became more important while the selection of beam energy did not have a significant effect. These findings motivate further development to ensure direct mappings of accurate image data into dose-responses, and to ensure a high spatial certainty of the tumor positioning when implementing DPBN in a clinical setting.

Disclosure statement

Erik Traneus is employed by RaySearch Laboratories AB.
The other authors declare no conflict of interest.

Funding

This research was supported by the Swedish Cancer Society, grant number 130632. We are grateful to Mikael Bylund and Karin Söderkvist at Umeå University Hospital for helping with the collection of patient data.

ORCID

Eric Grönlund http://orcid.org/0000-0002-4603-6338
Erik Almhagen http://orcid.org/0000-0001-8661-4019
Silvia Johansson http://orcid.org/0000-0002-4446-796X
Erik Traneus http://orcid.org/0000-0002-1850-7382
Tufve Nyholm http://orcid.org/0000-0002-8971-9788
Camilla Thellenberg http://orcid.org/0000-0002-7061-7255
Anders Ahnesjö http://orcid.org/0000-0001-8265-4785

References

[1] Möller TR, Brorsson B, Ceberg J, et al. A prospective survey of radiotherapy practice 2001 in Sweden. Acta Oncol. 2003;42(5–6):387–410.
[2] Widmark A, Klepp O, Solberg A, et al. Endocrine treatment, with or without radiotherapy, in locally advanced prostate cancer (SPCG-7/SFUO-3): an open randomised phase III trial. Lancet. 2009;373(9660):301–308.
[3] Pollack A, Zagars GK, Starkschall G, et al. Prostate cancer radiation dose response: results of the MD Anderson phase III randomized trial. Int J Radiat Oncol Biol Phys. 2002;53(5):1097–1105.
[4] Zietman A, DeSilvio M, Slater J, et al. Comparison of conventional-dose vs high-dose conformal radiation therapy in clinically localized adenocarcinoma of the prostate. JAMA. 2005;294(10):1233–1239.
[5] Peeters STH, Heemsbergen WD, Koper PCM, et al. Dose-response in radiotherapy for localized prostate cancer: results of the dutch multicenter randomized phase III trial comparing 68 Gy of radiotherapy with 78 Gy. J Clin Oncol. 2006;24(13):1990–1996.
[6] Dearnaley DP, Sydes MR, Graham JD, et al. Escalated-dose versus standard-dose conformal radiotherapy in prostate cancer: first results from the MRC RT01 randomised controlled trial. Lancet Oncol. 2007;8(6):475–487.
[7] Zelefsky MJ, Pei X, Chou JF, et al. Dose escalation for prostate cancer radiotherapy: predictors of long-term biochemical tumor control and distant metastases–free survival outcomes. Euro Urol. 2011;60(6):1133–1139.
[8] Morris WJ, Tyldesley S, Rodda S, et al. Androgen suppression combined with elective nodal and dose escalated radiation therapy (the ASCENDE-RT Trial): an analysis of survival endpoints for a randomized trial comparing a low-dose-rate brachytherapy boost to a dose-escalated external beam boost for high- and intermediate-risk prostate cancer. Int J Radiat Oncol Biol Phys. 2017;98(2):275–285.
[9] Arrayeh E, Westphalen AC, Kurhanewicz J, et al. Does local recurrence of prostate cancer after radiation therapy occur at the site of primary tumor? Results of a longitudinal MRI and MRSI study. Int J Radiat Oncol Biol Phys. 2012;82(5):e787–e793.
[10] Beckendorf V, Guerif S, Le Prisé E, et al. 70 Gy versus 80 Gy in localized prostate cancer: 5-year results of GETUG 06 randomized trial. Int J Radiat Oncol Biol Phys. 2011;80(4):1056–1063.
[11] Ling CC, Humm J, Larson S, et al. Towards multidimensional radiotherapy (MD-CRT): biological imaging and biological

conformality. International Journal of Radiation Oncology*Biology*Physics. 2000;47(3):551–560.
[12] Epstein JI, Zelefsky MJ, Sjoberg DD, et al. A contemporary prostate cancer grading system: a validated alternative to the gleason score. Eur Urol. 2016;69(3):428–435.
[13] Magi-Galluzzi C, Montironi R, Epstein JI. Contemporary gleason grading and novel grade groups in clinical practice. Curr Opin Urol. 2016;26(5):488–492.
[14] Han M, Partin AW, Zahurak M, et al. Biochemical (prostate specific antigen) recurrence probability following radical prostatectomy for clinically localized prostate cancer. J Urol. 2003;169(2): 517–523.
[15] Loeb S, Folkvaljon Y, Robinson D, et al. Evaluation of the 2015 Gleason grade groups in a nationwide population-based cohort. Eur Urol. 2016;69(6):1135–1141.
[16] Ghobadi G, de Jong J, Hollmann BG, et al. Histopathology-derived modeling of prostate cancer tumor control probability: implications for the dose to the tumor and the gland. Radiothe Oncol. 2016;119(1):97–103.
[17] Turkbey B, Shah VP, Pang Y, et al. Is apparent diffusion coefficient associated with clinical risk scores for prostate cancers that are visible on 3-T MR images? Radiology. 2011;258(2):488–495.
[18] Tamada T, Sone T, Jo Y, et al. Apparent diffusion coefficient values in peripheral and transition zones of the prostate: comparison between normal and malignant prostatic tissues and correlation with histologic grade. J Magn Reson Imaging. 2008; 28(3):720–726.
[19] Shigemura K, Yamanaka N, Yamashita M. Can diffusion-weighted magnetic resonance imaging predict a high gleason score of prostate cancer? Korean J Urol. 2013;54(4):234.
[20] deSouza NM, Riches SF, VanAs NJ, et al. Diffusion-weighted magnetic resonance imaging: a potential non-invasive marker of tumour aggressiveness in localized prostate cancer. Clin Radiol. 2008;63(7):774–782.
[21] Bittencourt LK, Barentsz JO, de Miranda LCD, et al. Prostate MRI: diffusion-weighted imaging at 1.5T correlates better with prostatectomy Gleason grades than TRUS-guided biopsies in peripheral zone tumours. Eur Radiol. 2012;22(2):468–475.
[22] Mazaheri Y, Hricak H, Fine SW, et al. Prostate tumor volume measurement with combined T2-weighted imaging and diffusion-weighted MR: correlation with pathologic tumor volume 1. Radiology. 2009;252(2):449–457.
[23] Boesen L, Chabanova E, Løgager V, et al. Apparent diffusion coefficient ratio correlates significantly with prostate cancer gleason score at final pathology: ADC_{ratio} Correlates with Gleason Score. J Magn Reson Imaging. 2015;42(2):446–453.
[24] Grönlund E, Johansson S, Nyholm T, et al. Dose painting of prostate cancer based on Gleason score correlations with apparent diffusion coefficients. Acta Oncol. 2018;57(5):574–581.
[25] Vogelius IR, Bentzen SM. Meta-analysis of the Alpha/Beta ratio for prostate cancer in the presence of an overall time factor: bad news, good news, or no news? Int J Radiat Oncol Biol Phys. 2013; 85(1):89–94.
[26] Casares-Magaz O, van der Heide UA, Rørvik J, et al. A tumour control probability model for radiotherapy of prostate cancer using magnetic resonance imaging-based apparent diffusion coefficient maps. Radiother Oncol. 2016;119(1):111–116.
[27] Fredriksson A, Forsgren A, Hårdemark B. Minimax optimization for handling range and setup uncertainties in proton therapy: minimax optimization for handling uncertainties in proton therapy. Med Phys. 2011;38(3):1672–1684.
[28] Unkelbach J, Alber M, Bangert M, et al. Robust radiotherapy planning. Phys Med Biol. 2018;63(22):22TR02.
[29] Kotte ANTJ, Hofman P, Lagendijk JJW, et al. Intrafraction motion of the prostate during external-beam radiation therapy: analysis of 427 patients with implanted fiducial markers. Int J Radiat Oncol Biol Phys. 2007;69(2):419–425.
[30] Monninkhof EM, van Loon JWL, van Vulpen M, et al. Standard whole prostate gland radiotherapy with and without lesion boost in prostate cancer: toxicity in the FLAME randomized controlled trial. Radiother Oncol. 2018;127(1):74–80.
[31] Lips IM, van der Heide UA, Haustermans K, et al. Single blind randomized phase III trial to investigate the benefit of a focal lesion ablative microboost in prostate cancer (FLAME-trial): study protocol for a randomized controlled trial. Trials. 2011;12:255.
[32] Borren A, Groenendaal G, Moman MR, et al. Accurate prostate tumour detection with multiparametric magnetic resonance imaging: dependence on histological properties. Acta Oncologica. 2014;53(1):88–95.
[33] Sterpin E, Differding S, Janssens G, et al. Generation of prescriptions robust against geometric uncertainties in dose painting by numbers. Acta Oncol. 2015;54(2):253–258.
[34] Witte MG, Shakirin G, Houweling A, et al. Dealing with geometric uncertainties in dose painting by numbers: introducing the ΔVH1This work was supported by Dutch Cancer Society grant 2007-3895.1. Radiother Oncol. 2011;100(3):402–406.
[35] Witte MG, J van der G, Schneider C, et al. IMRT optimization including random and systematic geometric errors based on the expectation of TCP and NTCP. Med Phys. 2007;34(9):3544–3555.